JOURNAL OF MATERIALS SCIENCE **36** (2001) 3573–3577

Mechanism of surface modification of a porous-coated Ti-6Al-4V implant fabricated by electrical resistance sintering

W. H. LEE*, S. J. KIM, W. J. LEE
Department of Advanced Materials Engineering, Sejong University, Seoul 143-747, Korea
E-mail: whlee@sejong.ac.kr

C. S. BYUN, D. K. KIM
Department of Materials Engineering, Taejon National University of Technology, Taejon 300-717, Korea

J. Y. KIM
Department of Semiconductor Engineering, Uiduk University, Kyongju 780-713, Korea

C. Y. HYUN
Department of Materials Science and Engineering, Seoul National University of Technology, Seoul 970-614, Korea

J. G. LEE
School of Metallurgical and Materials Engineering, Kookmin University, Seoul 136-702, Korea

J. W. PARK
Department of Metallurgical Engineering, Hanyang University, Seoul 133-791, Korea

A porous-coated Ti-6Al-4V implant was fabricated by electrical resistance sintering, using 480 μF capacitance and 1.5 kJ input energy. X-ray photoelectron spectroscopy (XPS) was used to study the surface characteristics of the implant material before and after sintering. There were substantial differences in the content of O and N between as-received atomized Ti-6Al-4V powders and the sintered prototype implant, which indicates that electrical resistance sintering alters the surface composition of Ti-6Al-4V. Whereas the surface of atomized Ti-6Al-4V powders was primarily TiO_2, the surface of the implant consisted of a complex of titanium oxides as well as small amounts of titanium carbide and nitride. It is proposed that the electrical resistance sintering process consists of five stages: stage I – electronic breakdown of oxide film and heat accumulation at the metal-oxide interface; stage II – physical breakdown of oxide film; stage III – neck formation and neck growth; stage IV – oxidation, nitriding, and carburizing; and stage V – heat dissipation. The fourth stage, during which the alloy repassivates, is responsible for the altered surface composition of the implant.

1. Introduction

The usual sequence in powder metallurgy operations is to compact a metal powder in a die at room temperature and subsequently sinter it at elevated temperatures. Not only are high pressure, high temperature, and long times required, but for reactive materials, such as Ti and its alloys, an inert atmosphere is also inevitably required. On the other hand, electrical resistance sintering, which is also known as electrodischarge compaction (EDC), combines compaction and sintering of powders by applying a high voltage and high density current, either with and without external pressure. Consolidation of the powder can be achieved in times as short as 300 μsec.

Okazaki *et al.* used this method to fabricate porous-coated Ti alloy implants [1]. They found that porosity and solid core size can be controlled by manipulating the capacitance and input energy [2]. Porous surfaces are intended to promote immobilization of the implant in bone by enabling mechanical interlocking between the implant and tissue, leading to osseointegration.

* Author to whom all correspondence should be addressed.

Compared to Ti implants fabricated by conventional hot pressing, sintering, and plasma spraying techniques [3–5], implants fabricated by electrical resistance sintering show superior physical and mechanical properties [2, 6].

In addition to the physical and mechanical properties, the surface properties of implants have been widely studied. Important surface characteristics of metallic biomaterials include the composition and structure of the surface oxide and contamination of the surface, which affect osseointegration and durability [7–11]. Recent studies demonstrate continued research into surface modification of Ti alloy for improving fatigue strength, wear resistance, and even corrosion resistance [12–19]. Typical methods for surface modification are thermal treatment and ion implantation. These treatments, however, are complex, time-consuming, and result in extra cost. Recently, Lee *et al.* found that electrical resistance sintering causes formation of TiN and TiC in addition to TiO_2 on the surface of a porous-coated Ti-6Al-4V implant [20]. The mechanism of this surface modification during electrical resistance sintering, however, has not been reported in detail. Therefore, the purpose of this paper is to provide a mechanistic explanation of the changes in surface characteristics of a porous Ti-6Al-4V implant fabricated by electrical resistance sintering.

2. Materials and methods

2.1. Ti-6Al-4V implant

As-received atomized Ti-6Al-4V powders, produced by the rotating electrode process (Goodfellow, Berwyn, PA), were sieved to yield one particle size class of 150–250 μm. The discharge conditions for sintering were a capacitance of 480 μF and a charge voltage of 2.5 kV, which yield an input energy of 1.5 kJ. The general preparative procedure has previously been described in detail [2, 20, 21]. An oscilliscope was used to monitor current and voltage throughout the discharge and sintering processes.

2.2. Surface analysis

As-received atomized Ti-6Al-4V powders and Ti-6Al-4V prototype implant were mounted on the spectrometer probe tip by means of double-sided adhesive tape and examined by XPS using a Kratos XSAM 800 spectrometer with Mg Kα (1.25 keV) radiation. The general XPS analytical procedure for obtaining survey and high resolution scans has previously been described in detail [20].

3. Results and discussion

General physical characteristics and mechanical properties of sintered 3.3 mm diameter Ti-6Al-4V implant prototype are listed in Table I [6]. The surface elemental concentrations for both as-received powders and porous implant as determined by XPS are listed in Table II. For both materials, C, O, and Ti were the main constituents with smaller amounts of Al and V also present. There were substantial differences in the content of O (41.34 at.% and 25.43 at.%) and N (0 at.% and 4.96 at.%) between as-received Ti-6Al-4V powders and prototype implant, respectively; the implant had a higher concentration of N but less O. Adventitious carbon, attributable to exposure to air, is normally detected on the surface of Ti and Ti-6Al-4V [22, 23]. In high resolution scans of the C1s region (not shown), an asymmetric peak with a maximum at 285 eV, mainly indicative of the C-H form, was observed for both materials. For the implant, a peak at the binding energy of 282.5 eV, which can be attributed to the formation of TiC, was also observed [20].

Additional high resolution scans revealed further differences regarding the surface chemical state of as-received Ti-6Al-4V powders and the prototype implant. Fig. 1 shows narrow scan spectra of the Ti 2p region for both materials. For the as-received powder, the Ti $2p_{3/2}$ peak at 459.2 eV, with 5.8 eV splitting between the Ti $2p_{1/2}$ and Ti $2p_{3/2}$, suggests a surface oxide in the form of TiO_2 [24]. A similar observation of TiO_2

TABLE I Physical characteristics and mechanical properties of a porous 3.3 mm electrical resistance sintered Ti-6Al-4V prototype implant (Each value was averaged over 5 implant samples, which has a standard deviation of ±3%) [6]

Core size (mm)	Neck size (μm)	Pore size (μm)	Compressive yield strength (MPa)	Ultimate strength (MPa)
2.24	45	121	328	420

TABLE II Surface composition of as-received Ti-6Al-4V powder and electrical resistance sintered Ti-6Al-4V prototype implant (Each value was averaged over 3 powder and implant samples, which has a standard deviation of ±2%)

	Concentration (at. %)	
Elements	As-received powders	Implant prototype
C	37.04	43.57
O	41.34	25.43
Ti	13.89	19.22
Al	6.26	6.07
V	1.46	0.76
N	0	4.96

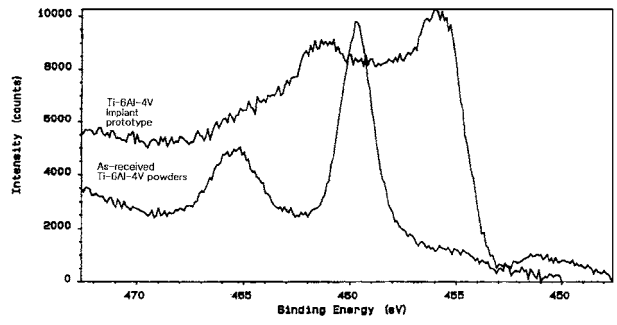

Figure 1 XPS high resolution narrow scan spectra of the Ti 2p region.

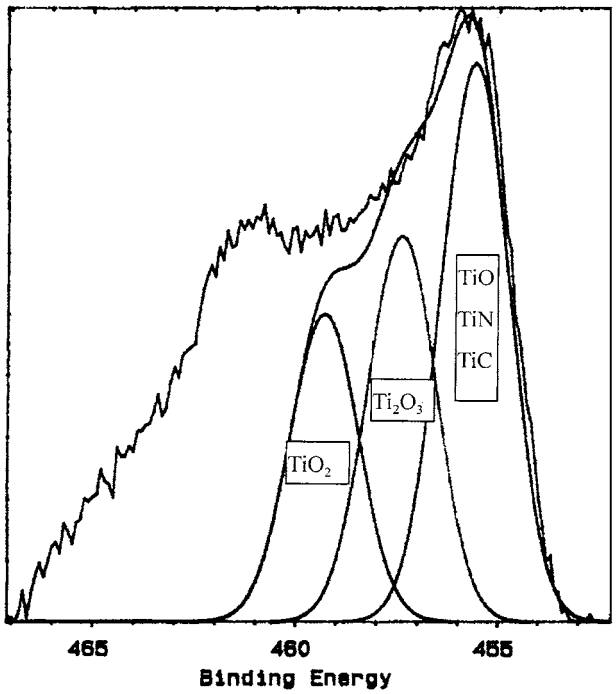

Figure 2 Deconvolution of the Ti 2p peak to show contributions of three major different functionalities.

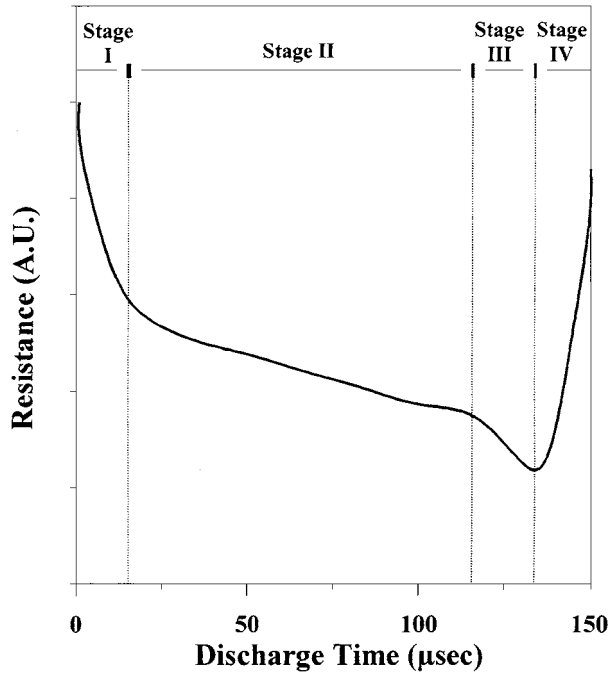

Figure 4 Resistance versus discharge time calculated from the voltage and current recordings.

on the surface of Ti and Ti alloys has been reported by several groups [25–28]. On the other hand, the electrical resistance sintered implant showed a Ti $2p_{3/2}$ peak at 455.7 eV, with 5.6 eV splitting between the Ti $2p_{1/2}$ and Ti $2p_{3/2}$ peaks. Furthermore, a high intensity region between Ti $2p_{1/2}$ and Ti $2p_{3/2}$ peaks resulted from an existence of Ti oxides was observed. The Ti 2p peak was therefore deconvoluted using a peak synthesis procedure that fits the measured peak to several Gaussian peaks. A typical deconvoluted XPS high resolution Ti 2p spectrum is shown in Fig. 2. It was found that the Ti 2p peak could be fitted with three major line shapes with peak binding energies of 459.2, 457.4, and 455.5 eV. These peaks were assigned to TiO_2, Ti_2O_3, and TiN and TiC, respectively. The presence of TiC on Ti-6Al-4V implant surfaces is supported by observation of a shoulder region at about 282.5 eV in the C1s narrow spectrum.

To elucidate the formation of TiN on the surface of the implant prototype, high resolution spectra of the N 1s region were obtained (Fig. 3) [20]. The maximum at 397.2 eV is identical to the N 1s position for nitride. This indicates the presence of a small amount of nitride and supports assignment of a TiN peak to the Ti 2p spectrum. From these results, it was known that the electrical resistance sintering process altered the surface composition of the as-received powders.

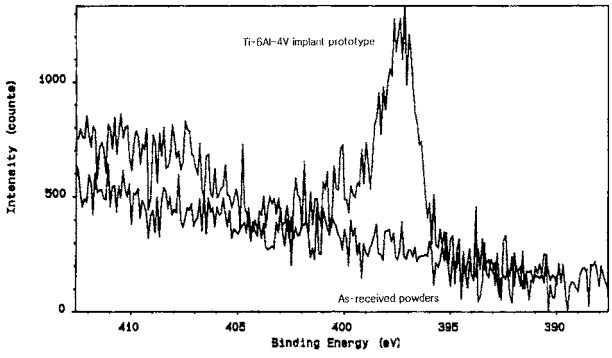

Figure 3 XPS high resolution spectra of the N 1s region of an electrical resistance sintered Ti-6Al-4V implant.

Fig. 4 shows the change in resistance through the powder column during discharge, which was calculated from the recordings of voltage and current. It can be seen that there are four distinct regions: 0 to 15 μsec for stage I; 15 to 120 μsec for stage II; 120 to 135 μsec for stage III; and 135 to 150 μsec for stage IV. In stage I, a rapid loss of resistance occurred. In stage II, the resistance decreased more slowly. In stage III, another rapid loss of resistance occurred, followed by a sudden increase of resistance in stage IV.

Davies *et al*., [29] proposed a three-stage mechanism for electrical resistance sintering. In the first stage, electronic breakdown of the oxide layer causes the rapid decrease in resistance, resulting in the formation of conducting layers. In the second stage, the formation and growth of conducting necks between particles occur simultaneously with the electromagnetic forces arising from the pinch effect [21]. This allows current to flow in the radial and azimuthal directions, leading to interconnection of powder particles. At this point, densification is promoted by the pinch forces generated in the whole powder column. In the third stage, the powder specimen acts like a porous solid conductor. No major changes in any physical properties occur.

On the other hand, Kim *et al.* [30] suggested a four-stage mechanism for electrical resistance sintering. They used 38–180 μm oxidized Ni powders. In the first stage, electronic breakdown of the oxide layer occurs, and heat accumulates at the metal-oxide interface. In the second stage, physical breakdown of oxide film occurs. Microstructural observation of particle-particle

interfacial regions by TEM showed an absence of oxide. In the case of a Ti-6Al-4V implant, microstructural examination of interfacial regions, such as necks and particle-particle interfaces, confirmed oxide film removal [2]. In the third and fourth stages, neck formation and growth and dissipation of energy through the conductive path, respectively, occur. The mechanism suggested by Kim *et al.* [30] is more acceptable, because the rapid drop in resistance at the early stage should take place by removal of resistive elements, such as oxide film, prior to the neck formation.

Neither group, however, reported a rapid increase of resistance after the final stage, III [29] or IV [30]. Even though the discharge time for the sintering is very short, elements in air, such as C, O, and N, are able to diffuse into the metal or chemisorb on the surface after physical breakdown of oxide film and neck formation. The elemental diffusion and/or chemisorption with subsequent oxidation, nitriding, and carburization of the reactive Ti would increase the resistance of the sintered powder column. Furthermore, the high current density results in movement of ions to result in multiple oxide forms, e.g., TiO_2 and Ti_2O_3. The rapid increase in resistance during stage IV (Fig. 4) can thus be attributed to the formation of new surface layer with different composition on the sintered powder column after breakdown of oxide layer and neck formation.

It is therefore concluded that the electrical resistance sintering process for the fabrication of a porous-coated Ti-6Al-4V implant consists of five stages. In the initial part of a discharge (0–15 μsec), electronic breakdown of oxide film and heat accumulation at the metal-oxide interface occur, resulting in a rapid loss of resistance. Between 15 and 120 μsec, physical breakdown of the oxide film causes a slow further decrease in resistance. Neck formation and neck growth, in the range of 120–135 μsec, cause another rapid loss of resistance by supplying conducting pathways. In the range of 135–150 μsec, repassivation of the alloy with formation of a new surface composition causes a rapid increase in resistance. In the final stage of a discharge, the residual heat in the sintered powders dissipates through the copper heat sink.

Numerous studies have demonstrated the importance of surface properties in determining biological responses to implants [7–11]. The altered surface composition on implants fabricated by electrical resistance sintering appears to be biocompatible and support rapid osseointegration [31]. The relationship between the surface chemical composition of the implant and the elemental concentrations in air is not clear. Future studies will examine controlling the surface composition of the implant following electrical resistance sintering by manipulating the sintering environment, such as by discharging in a sealed chamber and by changing the atmospheric composition, e.g., N_2 and/or O_2.

4. Conclusion

A mechanism was proposed to explain the altered surface chemistry of a porous-coated Ti-6Al-4V implants fabricated by electrical resistance sintering. In the early stage of discharge, the rapid loss of resistance occurs because of electronic breakdown of TiO_2 on the surface of atomized Ti-6Al-4V powders, and heat accumulates at the metal-oxide interface. In the second stage, sublimation of the metal layer beneath the oxide film causes further physical breakdown of Ti oxide film and a slow decrease in resistance. At this stage, the surface of the powder can be in the form of pure metals, such as Ti, Al, and V, without oxide. In the third stage, neck formation and growth result in the formation of conducting channels and cause another rapid loss of resistance. Subsequent repassivation of the alloy surface by reaction with atmospheric components to form TiO_2, Ti_2O_3, TiN and TiC cause a rapid increase of resistance. The residual heat transfers to the copper heat sink surrounding the Pyrex tube.

References

1. K. OKAZAKI, in "Report to National Science Foundation Novel Research Initiative Grant" (MSN-8610824, May 25, 1987).
2. K. OKAZAKI, W. H. LEE, D. K. KIM and R. A. KOPCZYK, *J. Biomed. Mater. Res.* **25** (1991) 1417.
3. K. ASAOKA, N. KUWAYAMA, O. OKUNO and I. MIURA, *ibid.* **19** (1985) 699.
4. S. YUE, R. M. PILLAR and G. C. WEATHERLY, *ibid.* **18** (1984) 1043.
5. R. M. PILLIAR, *ibid.* **21** (1987) 1.
6. W. H. LEE and J. W. PARK, *J. Mater. Sci. Lett.* **19**(11) (2000) 925.
7. B. KASEMO, *J. Prosth. Dent.* **49** (1983) 832.
8. B. KASEMO, J. LAUSMAA, P. I. BRANERMARK, G. A. ZARB and T. ALBREKTSSON, in "Tissue-Integrated Prostheses" (Quintessence Books, Chicago, 1985) p. 137.
9. K. GOMI and J. E. DAVIES, *J. Biomed. Mater. Res.* **27** (1993) 429.
10. J. Y. MARTIN, Z. SCHWARTZ, T. W. HUMMERT, D. M. SCHRAUB, J. SIMPSON, J. LAUKFORD, D. D. DEAN, D. L. COCHRAN and B. D. BOYAN, *ibid.* **29** (1995) 389.
11. B. GROESSNER-SCHREIBER and R. S. TUAN, *J. Cell Sci.* **101** (1992) 209.
12. T. MORITA, H. TAKAHASHI, M. SHIMIZU and K. KAWASAKI, *Fatigue Fract. Eng. Mater. Struct.* **20** (1997) 85.
13. J. E. LEMONS, *Surf. Coatings Techn.* **103/104** (1998) 135.
14. M. MORRA and C. CASSINELLI, *Surf. Intf. Analy.* **25** (1997) 983.
15. A. LOINAZ, M. RINNER, F. ALONSO, J. ONATE and W. ENSINGER, *Surf. Coatings Techn.* **103/104** (1998) 262.
16. H. PLENK, *J. Biomed. Mater. Res.* **43** (1998) 350.
17. C. HOWLETT, H. ZREIQAT, Y. WU, D. MCFALL and D. MCKENZIE, *ibid.* **45** (1999) 345.
18. T. CZERWIEC, H. MICHEL and E. BERGMANN, *Surf. And Coatings Techn.* **108/109** (1998) 182.
19. A. SARKISSIAN, A. BOURQUE-VIENS, R. PAYNTER, R. SAINT-JACQUES and B. STANSFIELD, *ibid.* **98** (1998) 1336.
20. W. H. LEE, J. W. PARK, D. A. PULEO and J. Y. KIM, *J. Mater. Sci.* **35**(3) (2000) 593.
21. W. H. LEE and D. A. PULEO, *J. Mater. Sci. Lett.* **18** (1999) 817.
22. T. HANAWA and M. OTA, *Appl. Surf. Sci.* **55** (1992) 269.
23. *Idem., Biomaterials* **12** (1991) 767.
24. J. MOULDER, W. STICKLE, P. SOBAL and K. BOMBER, "Handbook of X-ray Photoelectron Spectroscopy" (Perkin Elmer Corp., Eden Prairie, 1992) p. 213.
25. M. ASK, J. LAUSMAA and B. KASEMO, *Appl. Surf. Sci.* **35** (1989) 283.
26. N. R. ARMSTRONG and R. K. QUINN, *Surf. Sci.* **67** (1977) 451.
27. W. GOPEL, J. A. ANDERSON, D. FRANKEL, M. JAEHNIG, K. PHILLIPS, J. A. SHAFFER and G. ROCKER, *ibid.* **139** (1984) 333.

28. C. N. SAYERS and N. R. ARMSTRONG, *ibid.* **77** (1978) 301.
29. T. J. DAVIES and S. T. S. AL-HASSANI, "Advances in Materials Technology in America, Vol. 2, Materials Processing and Performance," edited by I. LeMay (America Society for Mechanical Engineers, New York, 1980) p. 147.
30. D. K. KIM, H.-R. PAK and K. OKAZAKI, *Mat. Sci. Eng.* **A104** (1988) 191.
31. J. F. DRUMMOND, J. T. DOMINICI, P. J. SAMMON, K. OKAZAKI, R. GEISSLER, M. I. LIFLAND, S. A. ANDERSON and W. RENSHAW, *J. Oral Implantol.* **21** (1995) 295.

Received 22 September 1999
and accepted 28 July 2000